Applied Catalysis B: Environmental 232 (2018) 472–480

Contents lists available at ScienceDirect

Applied Catalysis B: Environmental

journal homepage: www.elsevier.com/locate/apcatb

Dipyridylbenzene as a charming sensitizer to significantly enhance the photocatalytic activity of titanium dioxide

Heng Li[a,1], Meng Li[a,1], Lijun Zhang[a,*], Xiang Zhang[a], Yundi Ma[a], Bing Yu[a], Qiang Wei[b], Shuhua Yin[c]

[a] Tianjin Key Laboratory of Organic Solar Cells and Photochemical Conversion, School of Chemistry and Chemical Engineering, Tianjin University of Technology, Tianjin 300384, PR China
[b] Key Laboratory of Composite and Function Materials, School of Materials Science and Engineering, Tianjin University, Tianjin 300350, PR China
[c] Research and Development Department, Talent Biological Engineering Co. Ltd., Tianjin 300405, PR China

ARTICLE INFO

Keywords:
Hybrid materials
Photo degradation
Dye waste
Methyl orange
Titanium dioxide

ABSTRACT

Dipyridyl benzene skeleton (Py-ph-Py) was synthesized and chem.-grafted on titanium dioxide through hydrothermal method. The novel organic/inorganic hybrid structure DPA-TiO_2 displays remarkable photocatalytic activity and stability. The structural and surface characterization revealed that hybrid composites were linked with chemical ester bonds, which enabled the organic skeletons on the surface to act as charming transmitters of charges. The hybrid structure not only shortens the bond gap of catalyst hence to make charges be generated under visible light, but also transfers the photogenerated electrons in time to avoid them recombining with positive holes. In addition, the excellent adsorption capacity to waste organic compounds also contributes to its wonderful catalytic properties. The novel methodology is of great instructive to the utilization of solar energy to dispose environmental pollutions.

1. Introduction

The photocatalytic technology has been recently a hot research area, especially in the removal of environmental pollutants in aqueous phase as well as in gaseous media [1–5]. Many metallic oxides exhibit photocatalytic activities, which attributes to their semiconductor nature [6–8]. Such as titanium dioxide (TiO_2), one of the most potential semiconductor for degradation of unwanted organic compounds, can efficiently remove pollutants in contaminated water and air, and kill harmful bacteria in addition [9–11].

According to three major steps of photocatalytic reactions, i.e. (1) absorbing photons to generate electron-hole pairs on a semiconductor; (2) separating and migrating of electron-hole pairs; (3) taking place redox involving electrons and holes, the crucial factors determining the efficiency of photocatalysis are light absorption, charge separation and reaction kinetics, correspondingly, among which charge separation is the most important stage. When electrons (e^-) and holes (h^+) are generated at the surface of metallic oxides, they convert into excitons in quantum states near the surface after energy relaxation, during which a fast electron-hole recombination may take place to annihilate these charges, and so both electrons and holes are hardly transferred to substrate for redox reactions. Thus, to increase the photocatalytic activities, the photogenerated e^- and h^+ must be effectively separated into different positions of the catalyst [12,13].

So far, people have presented many methods to enhance charge separation or adsorption capacity to increase photocatalyst performance, among which hybridization has proved to be an effective one [14–21]. However, most of processes employed element doping or combining with inorganic metallic compounds, although they are effective sometimes, the desired catalyst preparation was hardly to be repeated and heavily in consuming energy during calcination stage.

Undisputedly, organic compounds are much versatile and easy to prepare, and have been widely investigated in photoelectrical materials [22,23]. Liu designed and synthesized an anatase TiO_2 based organic-inorganic hybrid photocatalyst which has hard cores (single-crystal TiO_2 nanocuboids) and soft shells (organic composites). The smart-joint organic layer (DMEA and LA) plays a crucial role in trapping Rhodamine B molecules and delivering them on the TiO_2 interfaces, thus displays superior RhB photodegradation performance [24]. Xu prepared a series of dye-modified TiO_2 photocatalysts using tolylene-2,4-diisocyanate (TDI) as a bridging molecule. Due to the existence of π-conjugated surface organic complexes, the as-synthesized

* Corresponding author at: 391 Binshui West Road, Xiqing District, Tianjin 300384, PR China.
E-mail addresses: cdlijun2002@126.com, cdlijun2002@tjut.edu.cn (L. Zhang).
[1] These authors contributed equally to this work.

https://doi.org/10.1016/j.apcatb.2018.03.096
Received 22 October 2017; Received in revised form 18 March 2018; Accepted 26 March 2018
Available online 27 March 2018
0926-3373/

photocatalysts exhibited much better activity under the visible light irradiation than bare TiO_2 [25].

For organic modifiers, a major hindrance to employ is itself degradation during photoreaction, which shortens the lifetime of photocatalysts. The key solution to this problem is using compounds with high anti-oxidation ability. However, it is not an easy job due to the high oxidation potential of photogenerated charges and initiated hydroxyl radicals, even electron-deficient pyridine skeleton cannot be spared [26,27]. Nevertheless, dipyridyl structures have been widely used both in photoelectrical and photocatalytic areas for their good stability [28–30], and they should be more stable under photocatalysis conditions when conjugated with benzene. Inspired by this idea, we designed a chem-linked hybrid photocatalyst, which dipyridyl benzene skeleton was employed as modifier for TiO_2. Our study shows that the modified TiO_2 exhibits a remarkable activity and stability in wide pH range of aqueous solutions. Under this hybrid catalyst, methyl orange (MO) can be photodegraded with small power consumption and within very short time. To the best of our knowledge, this is the first report about dipyridyl benzene skeleton enhancing the activity and stability of photocatalyst. Compared with the well-known noble metal cocatalysts (e.g., Pt, Au, Ag), the present easily obtained and cheap hybrid catalyst put forward an ideal and bright prospect in environmental photocatalysis and other relative areas. The work also provides a new insight for the potential photocatalytic applications of various organic and inorganic hybrid materials.

2. Experimental

2.1. Characterization

A field emission gun-scanning electron microscope (Zeiss Merlin Compact, Germany) operating at 5.0–10.0 kV was used to verify the material morphology. The X-ray powder diffraction data were collected from a Rigaku diffractometer (D/max 2500 PC, Japan) with a horizontal goniometer and CBO cross optical system, the powder samples were placed on zero background quartz sample holders and the XRD patterns were recorded at room temperature using Cu Kα radiation (k = 0.15406 nm). X-ray photoelectron (XPS) measurements were performed at a residual pressure of 10^{-9} mbar, using a Kratos Axis Ultra electron energy analyzer operating with an Al Kα monochromatic source. UV–vis spectrophotometer (Hitachi U3900, Japan) was used to test the photo absorbance of samples. FT-IR spectra were obtained using a Nicolet FT-IR spectrometer (Avatar 370, USA).

2.2. Preparation of organic modifiers

As illustrated in Scheme 1, ethyl tetracarboxylate and tetracarboxylic acid of dipyridylbenzene, which possess the properties of antioxidation and electron transmission, were synthesized with improved methods based on lit. [31].

Solvent-free synthesis of 1,4-dihydropyridine **1**: In a 50 mL round-bottomed flask, terephthalaldehyde (4.0 g, 0.03 mol), ethyl acetoacetate (15.63 g, 0.12 mol), and ammonium acetate (6.16 g, 0.08 mol) were charged and the mixture was heated to 120 ℃ to conduct Hantzsch reaction. After the completion of the reaction (confirmed by TLC, about 2.5 h), the mixture was cooled to 60 ℃ and poured into 50 mL ethanol, and after fully stirring, the precipitate was filtered and washed with ethanol three times, and then it was dried at 80 ℃ to give the pure pale yellow product **1** (16.14 g, 90%). ^{1}H NMR (400 MHz, $CDCl_3$) δ (ppm) 7.09 (s, 4 H, Ph-H), 5.56 (s, 2 H, NH), 4.95 (s, 2 H, dihydropyridine-CH), 4.09 (q, 8 H, J = 7.1 Hz, OEt), 2.33 (s, 12 H, Me), 1.21 (t, 12 H, J = 7.1 Hz, OEt).

Synthesis of 1,4-dipyridylbenzene **2**: A mixture of 1,4-dihydropridine **1** (16.65 g, 28.7 mmol) and 100 mL glacial acetic acid was placed in a 250 mL three-necked flask, while fully stirring at 65 ℃, sodium nitrite (5.94 g, 86.1 mmol) was added with three portions. After oxidation completion, the mixture was poured into 300 mL ice water mixture and neutralized with ammonia water. The precipitate was filtered and washed with water thoroughly to give the light yellow product **2** (15.40 g, 93%). ^{1}H NMR (400 MHz, $CDCl_3$) δ (ppm) 7.33 (s, 4 H, Ph-H), 4.10 (q, 8 H, J = 7.1 Hz, OEt), 2.63 (s, 12 H, Me), 1.18 (t, 12 H, J = 7.1 Hz, OEt).

Procedure for decarboxylation of pyridine ester **3**: A suspension of pyridine ester **2** (5.75 g, 10 mmol) in NaOH solution (40 mL, 30 wt %) and ethanol (150 mL) was heated to reflux at 80 ℃ till a clear liquid was formed. After ethanol was removed under vacuum, the mixture was then neutralized with diluted hydrochloric acid and its pH was adjusted to 3, the precipitate was filtered and washed with water thoroughly to give the earthy yellow product **3** (3.34 g, 72%). ^{1}H NMR (400 MHz, DMSO) δ (ppm) 7.36 (s, 4 H, Ph-H), 2.53 (s, 12 H, Me).

2.3. Preparation of hybrid catalyst DPA-TiO_2

Nano-TiO_2 P25 was purchased from Aladdin biochemical technology co.ltd. and was dried at 200 ℃ to recover its surface and get constant weight. The precise amount of compound **3** (see Table 1, discussion section) was added into 20 mL DMF and stirred to dissolve, and then 1 g TiO_2 was added, fully mixed, and sonicated (120 W, 40 kHz) 5 min to give a stable colloid. The colloid was then transferred into a 50 mL Teflon-lined autoclave. After heating and reacting at different conditions (see Table 1, discussion section), the resulting solid product was filtered and washed successively with DMF (1 × 10 mL), distilled water (3 × 20 mL), and ethanol (2 × 10 mL), then dried at 80 ℃ for 2 h to give modified catalyst DPA-TiO_2.

2.4. Degradation of methyl orange (MO)

As one of common dyes in the textile industry, MO aqueous solution was chosen as a typical organic waste. A 150 mL beaker was used as the reactor vessel, and the catalyst DPA-TiO_2 was added to the system containing MO solution (20 mg L^{-1}, 100 mL) under stirring. Lamp ① UV-365 nm, ZF-7A, 7 W/38 W, Gongyi Yuhua Instrument Co., Ltd. China; ② UV–vis 434 nm, Shanghai Jiguang special light Co., Ltd. China; ③ Xenon light, GX2300, 200 W, Shanghai Jiguang special light Co., Ltd. China.) was placed on the top of beaker (ca. 5 cm above the surface of the water) to provide light, and UV–vis absorption spectra were recorded at different intervals to monitor the degradation process. Before irradiation, two drops of 30 wt% H_2O_2 solution, about 0.04 mL, were added into solution to trigger the creation of radicals, and the pH values of the systems was adjusted with 0.1 M HCl solution and 0.1 M sodium hydroxide solution. Comparing experiments in the promotion of TiO_2 under other same conditions as DPA-TiO_2 was also performed in order to assess catalyst property.

As for the photocatalytic decolorization of dilute MO aqueous solution is a pseudo-first-order reaction, its kinetics may be expressed as $\ln(c_0/c) = k\,t$, where k is the apparent rate constant, and c_0 and c are the methyl orange concentrations before and after irradiation for t min, respectively [32]. At regular intervals, samples were taken out to be immediately filtrated and estimated by measuring the maximum absorbance at 463 nm using an UV–vis spectrophotometer (721 UV–vis spectrophotometer, Shanghai Youke Instrument Co., Ltd. China). The degradation rate (DR) of MO was calculated according to the equation $DR\ (\%) = 100 \times (C_0 - C_t)/C_0$, where DR is the degradation rate of MO after irradiation for t minutes, and C_t is the concentration of MO after irradiation for t minutes, and C_0 is the initial concentration of MO.

3. Results and discussion

3.1. Preperation conditions of organic-inorganic hybrid catalyst

To obtain organic-inorganic hybrid photo-catalyst DPA-TiO_2 with high activity, selectivity and stability, the preparation conditions

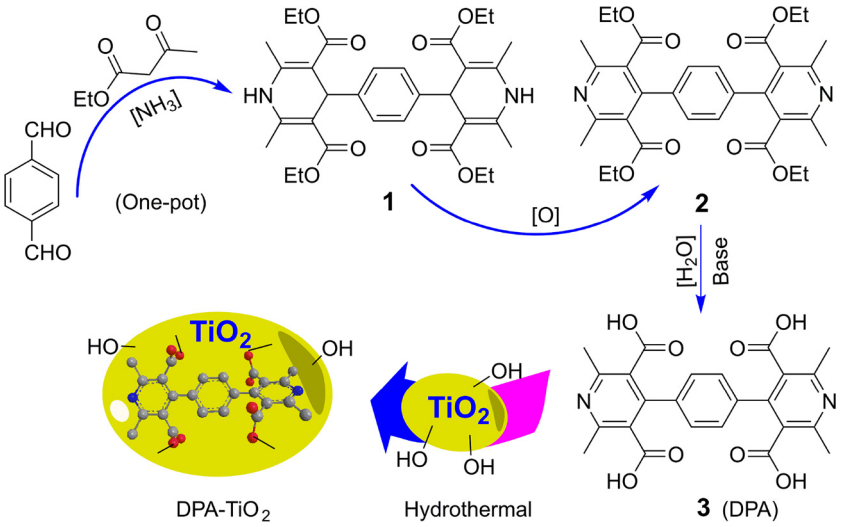

Scheme 1. Synthetic route of DPA and DPA-TiO_2.

Table 1
Preparation conditions of catalyst DPA-TiO_2[a].

Entry	Solvent	DPA amount (g)	Temperature (°C)	Time (h)	DR (%)[b]	Stability (times)[c]
1	EH[d]	0.1	120	4	40.3	–
2	DMF	0.1	160	4	83.5	3
3	DH [e]	0.1	200	4	82.1	1
4	EH	0.1	160	8	54.6	–
5	DMF	0.1	200	8	98.7	7
6	DH	0.1	120	8	69.2	–
7	DMF	0.1	120	12	68.5	–
8	DH	0.1	160	12	81.6	1
9	DMF	0.05	200	8	84.4	7
10	DMF	0.2	200	8	97.5	7
11	DMF	0.3	200	8	97.4	7

[a] 1 g of TiO_2 was used for each entry to prepare DPA-TiO_2. In property experiments, 0.1 g/L DPA-TiO_2 was used and the initial pH of MO solution is adjusted to 6 with 0.1 M hydrochloric acid.

[b] Degradation rate (DR) is the relative rate of reduction of MO concentration after 30 min irradiation (the wavelength of main peak is 434 nm).

[c] Stability is assessed with the reused times of catalyst which each one is under pH = 6 and 30 min UV–vis irradiation, and the last DR is not less than 90%.

[d] EH = EtOH + H_2O (volume ratio is 5 : 1). It was not used at 200 °C in case of safety.

[e] DH = DMF + H_2O (volume ratio is 10 : 1).

including hydrothermal solvents, temperature and time were first optimized, and the results were listed in Table 1. Besides using DR of MO to determine the optimal conditions, the reuse times of catalyst DPA-TiO_2 listed in the last column were also used as another important criterion.

It can be seen from Table 1 that the mixture of ethanol and water is not a good hydrothermal solvent for the preparation of target catalyst. It only gave 54.6% DR when the catalyst was prepared at 160 °C for 8 h in EH (Table 1, Entry 4), while at lower temperature 120 °C it decreased to 40.3% DR (Table 1, Entry 1), which is almost matched with the performance of naked TiO_2. These results indicate that compound **3** was not fixed well on the surface of TiO_2, which probably because of the hindrance of hydroxyl of ethanol to esterification reaction. Evidently, DMF as a good solvent for compound **3**, gave much better results than ethanol. However, the addition of water to DMF decreased the performance of catalysts (Table 1, Entry 3, 6, and 8). The best catalyst, which was prepared at 200 °C for 8 h in DMF, gave excellent DR 98.7% (Table 1, Entry 5), which is 2.5 times more than that of naked TiO_2. Thus DMF was utilized for the preparation of catalyst DPA-TiO_2. From Table 1, it can be concluded that the optimal dosage of DPA is 0.1 g as to 1 g TiO_2. The limited hydroxyl groups on the surface of TiO_2 may be account for this low loading of DPA.

3.2. Catalyst structure and its stability

3.2.1. FT-IR spectrum

The organic-inorganic hybrid DPA-TiO_2 was first identified with FT-IR spectrum. It can be seen from Fig. 1 that the IR of DPA-TiO_2 gave obvious organic peaks, especially at the region from 1000 cm^{-1} to 1800 cm^{-1}, which demonstrated the successful bonding DPA on TiO_2. There are evident changes compared with the IR of DPA. The DPA carbonyl stretching vibration of 1734.06 cm^{-1} was divided into two strong peaks at 1698.34 cm^{-1} and 1653.75 cm^{-1}, and the stretching vibration of methyl at 2982 cm^{-1}, and also methylene at 2941 cm^{-1}, became weaker in DPA-TiO_2. These gave enough information that the esterification reaction, as illustrated in Scheme 1, had happened between DPA and TiO_2. From Fig. 1, we can also find out the charming stability of DPA-TiO_2, which its structure remains no change after being reused for 6 times. It is obviously that the chemical linkage of DPA and TiO_2 stabilized the structure; this proved that organic molecules could be fixed on the surface of TiO_2 through chemical reactions, and this chemical fixation prevents the bonded organic compounds from photodegradation.

3.2.2. Thermal and BET analysis

TG (40–800 °C) with a heating rate of 10 °C/min^{-1} in air was carried

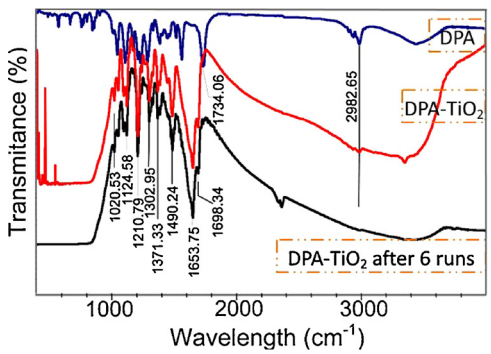

Fig. 1. FT-IR of DPA, DPA-TiO_2, and DPA-TiO_2 after being 6 times reused.

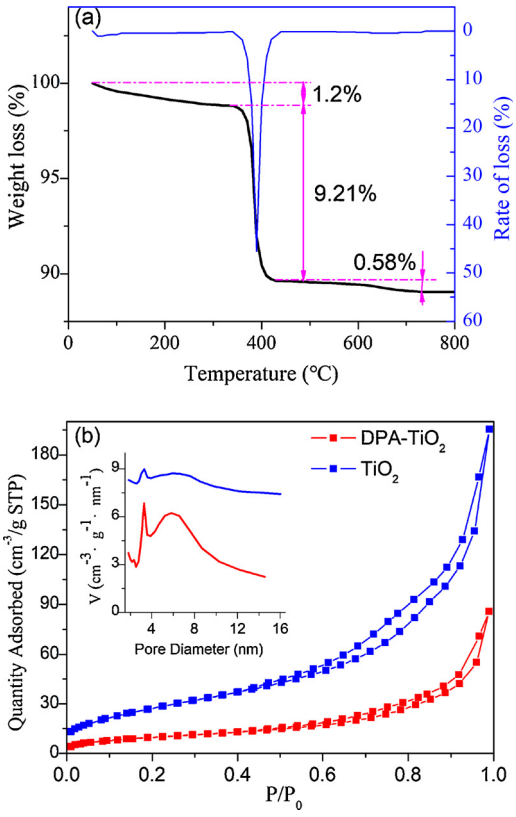

Fig. 2. TG (a) and BET (b) analysis of DPA-TiO_2 and TiO_2. The inserted is the BJH dV/dD pore volume distribution of DPA-TiO_2 (red line) and TiO_2 (blue line). BET surface area of TiO_2 and DPA-TiO_2 is 103.3263 ± 0.5486 m^2/g and 35.9029 ± 0.1335 m^2/g, respectively. (For interpretation of the references to colour in this figure legend, the reader is referred to the web version of this article).

out to determine the phase transition of DPA-TiO_2. As illustrated in Fig. 2, the weight of DPA-TiO_2 gradually reduced along with the increase of calcination temperature. Before 350 ℃, it gave 1.2% weight loss due to the removal of the adsorbed water molecules [33]. The abrupt weight loss (9.21%) occurred in the range of 355 ℃ to 410 ℃, which can be attributed to the decomposition of DPA from TiO_2 surface. This lost mass is coincident with the previously stated loading amount of DPA. Further weight loss in higher calcinations temperature can be attributed to the dehydroxylation by removal of structural OH units of titanium oxide [34]. BET analysis was conducted at −195.850 ℃ with TriStar II 3020 3.02 of Micromeritics Instrument Corporation. It can be seen from Fig. 2(b) that

comparing with TiO_2, the surface area and pore volume of DPA-TiO_2 decreased obviously, and its distribution of pore volume became narrower. The change of BET surface of DPA-TiO_2 testified the success of DPA loading on TiO_2, but also indicated a declining result of adsorption property which seems against to the measured data (presented latter) of its dye adsorption in water. The distinction of organic and inorganic absorbates should be account for this case, in fact, DPA not only changed the surface species but also the surface nature of TiO_2, both in polarity and in dielectricity, thus enhanced the adsorption capacity to organic dyes.

3.2.3. XRD, SEM and TEM features

The crystallization of solid maters often gives important structural information, especially for the existence state of loading molecules [35]. Thus powder DPA-TiO_2 and TiO_2 were tested with X-ray diffraction (XRD), and the result was presented as Fig. 3. Obviously, all Bragg peaks of Fig. 3 are consistent with anatase phase (JCPDS no.21-1272) [36], which shows peaks at 25.14° (101), 37.88° (004), 47.98° (200), 53.86° (105), 55.0° (211), 62.66° (204). For no additional peaks appear at DPA-TiO_2 sample, it may suggest that DPA molecules be chemically fixed on the surface of TiO_2, and the partial loading of these organic molecules do not influence the crystallization of solid supporters. However, the intensity of the XRD diffraction peaks of DPA-TiO_2 decreases evidently perhaps for the shelter effect of DPA, which therefore interprets the lower photocatalysis activity was observed when the loading amount of DPA on TiO_2 was higher than 0.1 g/g (see Table 1).

The SEM images of DPA-TiO_2 and TiO_2 were tested with field emission scanning electron microscopy (FESEM, ZEISS MERLIN Compact) using 5 kV. Fig. 3(b) and (c) shows the morphologies of TiO_2 and DPA-TiO_2, respectively. Although the later displays more aggregated than the former, they all show largely same morphology with average crystal size of 25 nm. Further microscopic test was carried out on HRTEM (JEM2100-PLUS, Japan) and presented as Fig. 3(d)–(f). It was shown in Fig. 3(d) that TiO_2 nanoclusters covered with organic compound, and the morphology of TiO_2 was easy to be observed for transparent DPA to some extent. The same feature can also be observed in Fig. 3(e) that DPA evenly doped on the surface of TiO_2. The mainly anatase particles can be observed in Fig. 3(f) which is coincident with its XRD features.

3.2.4. XPS characterization

In order to identify organic/inorganic interactions, XPS spectrum of DPA-TiO_2 was tested and selectively shown in Fig. 4. The C1s peak was fitted into four peaks for C—C, C—O, C═O, and C—O—Ti at 284.6, 286.2, 288.0, and 289.1 eV, respectively [37]. This is consistent with previously discussed IR spectra, which clearly shows the bonding interaction of DPA and TiO_2. The case can also be speculated from O1s spectrum, which shows Ti-O, C—O—Ti or C═O, and C—O at 529.7, 531.3, and 532.4 eV, respectively [38].

3.2.5. UV–vis characterization and electrochemical analysis

The successful loading of DPA on TiO_2 can be further demonstrated by UV–vis spectra, as shown in Fig. 5(a). As an indirect-bandgap semiconductor, the bandgap between the conduction band and valence band can be estimated from UV–vis measurements. These UV–vis data were reformed to a plot of $(Ahv)^2$ against *Energy* in Fig. 5(a) to deduce the bandgap of catalyst, where A is UV–vis absorbance, and $hv = (1240/wavelength)$. Obviously, compared with TiO_2, the UV light absorption intensity of hybrid catalyst was greatly enhanced on account of the fixation of DPA, and a new evident peak appeared at 382 nm which can be attributed to the new transition state initiating from the bonding of DPA and TiO_2. Its band egde of optical absorption reaches visible region, which suggests the catalyst can be used under visible light. It is obtained from extrapolated plot (purple dashed line) that the bandgap of TiO_2 is 3.2 eV, which is consistent with that reported for anatase nano-TiO_2 [39,40]. After modified with DPA, it exhibits an extraploted bandgap at 2.82 eV, which is less than 2.98 eV of DPA, this probably suggests a new heterojunction formed between organic and inorganic molecules, and this new formed surfacial structure is then named as DPE for it is the ester product of esterafication of DPA and TiO_2. Obviously, this bandgap helps excitation wavelength move to visable light. That is why the best performance of catalyst was presented under 434 nm lamp.

In electrochemical analysis, a three-electrode cell with an electrochemical analyzer (CH1660E, Shanghai Chenhua Co.LTD) was used. The working electrode was prepared through coating FTO glass with the slurry (15 μL) of catalysts (Alcoholic dispersion: 20 m g catalyst was fully dispersed in 1 mL EtOH with 40 kHz ultrasonication.) and annealed at 473 K for 1 h. Using 0.1 M Na_2SO_4 (pH 6.9) as electrolyte solution, and a Pt sheet and a Ag/AgCl electrode as the counter and reference electrodes, respectively, Mott—Schottky analysis was conducted at 10 mV perturbation signal and the results were presented in Fig. S6. It can be seen from Fig. S6 that the positive slope of streight line

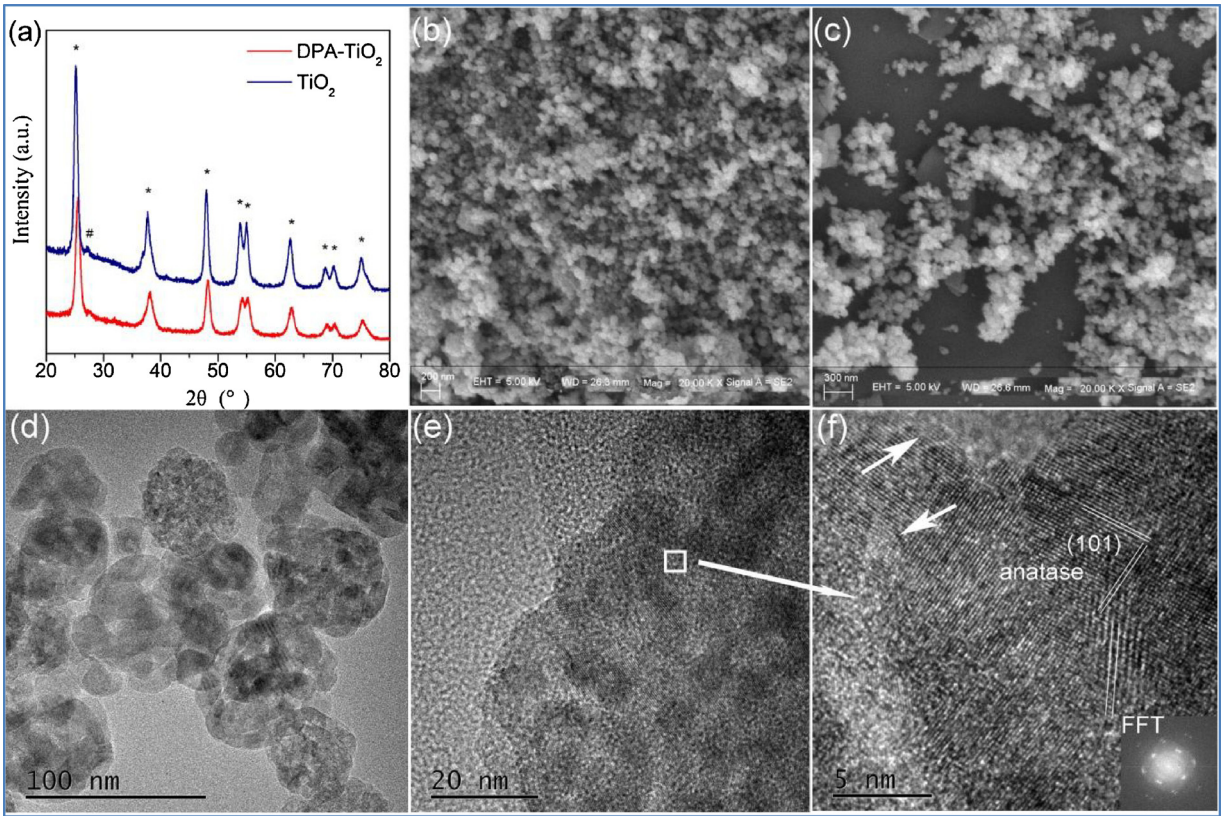

Fig. 3. Surface features of catalysts. (a) XRD features of DPA-TiO_2 and TiO_2. (b) HRSEM features of TiO_2. (c) HRSEM features of DPA-TiO_2. (d)–(f) HRTEM features of DPA-TiO_2 (The inserted is the FFT photo).

determines DPA-TiO_2 to be still a n-type semiconductor, and its CB bottom is -0.37 V (vs NHE, pH 0), which is lower than 0.09 V (vs NHE, pH 0) of TiO_2. This is consistent with the phenomena of photocatalysis and the former remarks about UV–vis spectra, and also gives a reliable support for subsequent analysis of mechanism. In photo current test, 0.25 cm^2 area of the working electrode was exposed to the irradiation at $\lambda > 300$ nm at a bias potential of 0.5 V. As shown in Fig. 5(b), the photocurrent density on DPA-TiO_2 is higher than that on TiO_2, this suggests that DPA enhances charge separation and promotes the photocatalytic properties.

3.3. Photodegradation properties of DPA-TiO_2

3.3.1. Adsorption properties of catalysts

It is well known that sufficient contact of organic pollutants with photocatalysts is a key element of the photocatalysis [41]. Quick adsorbing organic pollutants is an important advantage of fixing organic cocatalyst on the surface of TiO_2, as the photocatalytic reactions occur on the surface of catalysts. Thus equilibrium adsorption of MO on different catalysts was firstly tested and shown in Fig. 6(a). Clearly, except much low pH condition, which both TiO_2 and DPA-TiO_2 exhibit absolutely adsorption of MO as for the consecutive linking of MO quinoid molecules (Fig. S4), DPA-TiO_2 exhibits much higher adsorption capacity of MO than anatase TiO_2 in the wide range of pH from 3 to 10. Especially near neutral conditions, the differences of their adsorption capacity are more significant (72.6% of DPA-TiO_2 to 12.3% of TiO_2). The high adsorption ability may be attributed to the flexible interactions of DPA with MO. As illustrated in Fig. S5, the interactions of DPA and MO may include head-head ionic binding (sulfo group with pyridine segment under acidic condition), N—HN hydrogen bonds (diazo group with pyridine segment), π-π interactions (benzene and pyridine planes of DPA with benzene planes of MO) and other polar interactions initiated by oxygen atoms of DPA. Although some interactions such as ionic bindings of sulfo group and pyridine segment exist in acidic condition, other interactions can guarantee good adsorption of DPA to MO under wide pH scope. It is very important that DPA-TiO_2 exhibits excellent adsorbability to waste dye in near neutral conditions, for most of dye waste water was discharged by plants in this pH scope.

3.3.2. Inflence of light types on DR of MO

The nature of light is an important factor for photodegradation. Thus 30 mg/L of MO aqueous solution was first used to degrade under different kind of lights. The removal result of MO with DPA-TiO_2 was shown in Fig. 6(b). Evidently, with no light, the degradation rate of MO in 60 min was only 7.6%. While with 38 W of mercury lamp (illuminance 680 lx., main peak $\lambda\rho = 434$ nm, light power 593 $\mu w/cm^{-2}$), which its light wavelength meets the first bandgap of catalyst, DR was increased remarkably to 99.8% in 30 min. When a 200 W xenon lamp with optical filter to block UV light was employed (11300 lx, main peak $\lambda\rho = 760$ nm, light power 4944 $\mu w/cm^{-2}$), the DR was slowly increased to 92.5% after 60 min. Although it is lower than that of 38 W mercury lamp (that with UV and visible light) and high in energy consumption, splendid visible photocatalytic activity of DPA-TiO_2 was demonstrated. The red shift of modified TiO_2 in absorbing light brings its good performance in a wide range of wavelength. Near UV light was also utilized to compare DPA-TiO_2 and TiO_2. Under 7 W of 365 nm UV lamp (light power 78.96 $\mu w/cm^{-2}$), the former gave 78.6% DR of MO after 60 min illumination, which is much higher than the later with near 60% DR. These results demonstrated that the photoactivity of TiO_2 was greatly enhanced by chem.-grafting of DPA, and the energy consumption was significantly decreased.

3.3.3. Influence of solution pH on DR

MO displays two different chemical structures depending on solution acidity [42], hence its DR under light was much influenced by pH. Fig. 6(c) shows the influence of pH on DR. Clearly, DR of MO in acidic

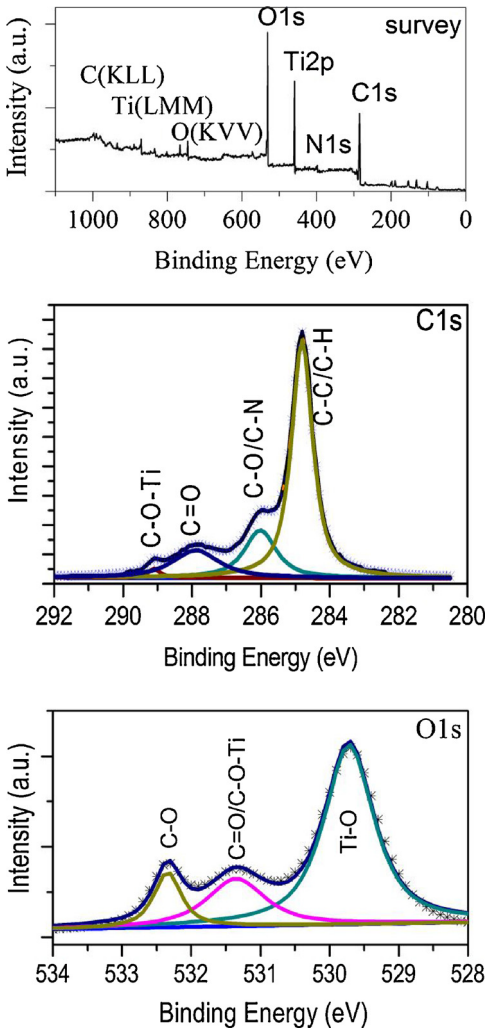

Fig. 4. XPS spectrum of DPA-TiO_2.

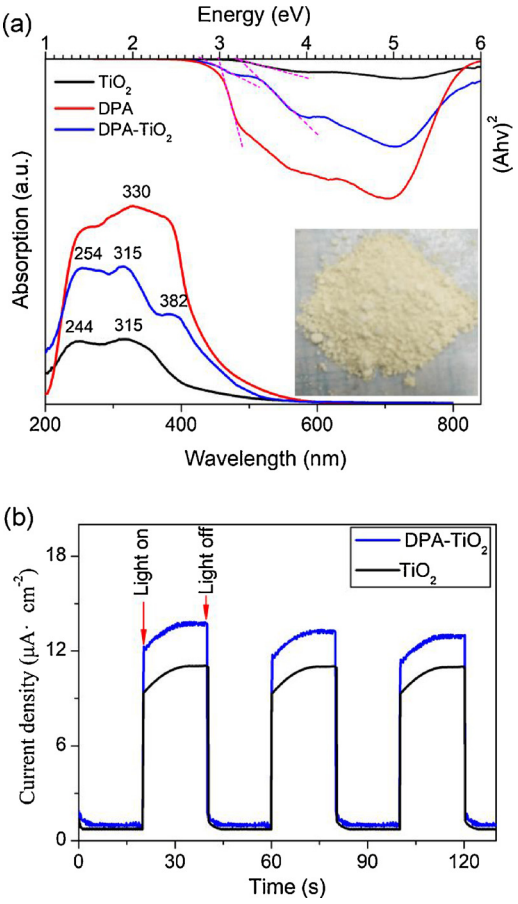

Fig. 5. (a) UV–vis spectra and bandgap plots of TiO_2, DPA and DPA-TiO_2. The inserted photo is DPA-TiO_2 sample. (b) Photocurrent response of TiO_2 and DPA-TiO_2 under $\lambda > 300$ nm irradiation (0.5 V bias). (For interpretation of the references to colour in the text, the reader is referred to the web version of this article.)

conditions was better than that in basic solutions. DPA plays an important role in this process. Before loading of DPA, DR decreases quickly under TiO_2 catalysis as the pH values increased, which is consistent with the previous researches [43]. When TiO_2 was modified with DPA, the difference of DR under acidic and neutral conditions was shortened evidently, thus the sufficient removal of MO can be fulfilled under near neutral conditions. In basic solutions, both catalysts display declining capacity, still DPA-TiO_2 gave much higher DR than TiO_2. It is well known that the surfaces of TiO_2 become negatively charged with pH increasing, which will go against the adsorption of anionic MO molecules because of electrostatic repulsion. This is why TiO_2 gave bad performance under basic conditions, while the modified TiO_2 absorbs MO through other interactions, which guarantees its good adsorption capacity.

3.3.4. Influence of the concentration of MO and the dosage of DPA-TiO_2 on DR

The influence of the initial MO concentration on DR was investigated by changing MO concentrations from 10 to 120 mg/L. As illustrated in Fig. 6(d), with the increasing of the concentration of MO, DR decreased gradually, but the change is very limited. Many researchers have declared that at higher concentration, dye MO solution blocks light wave to go into its inside for its heavy color and thus DR decreased quickly. The most probable reason for this case is that they conducted their tests under strong acidic conditions, in which MO displays its heavy red color. Whereas our catalyst was used in near neutral conditions where MO shows yellow color, hence the blocking effect is smaller. In addition, DPA-TiO_2 can quick decrease the free MO molecules through its fast adsorption and degradation capacity, and so DR was not much influenced by dye concentration. This indicates a high catalytic capacity of DPA-TiO_2 in dye degradation reactions and potential for practical application. Fig. 6(d) also shows the optimal usage of DPA-TiO_2 which is around 0.1 g/L when the concentration of MO is 30 mg/L. The lower dosage provides small area of catalyst surface that is not enough for efficiently absorbing MO molecules, while the higher usage such as 0.15 g/L is extravagant for it did not evidently increase DR.

3.3.5. Reusability of DPA-TiO_2

In the experiments, DPA-TiO_2 exhibited high stability which may be attributed to its changes among different structural types. As shown in Fig. 7(a), its dihydropyridine type and pyridine type possess high antioxidant property, and its pyridine oxide type display important role in the transmission of charges. The three types can interconvert in redox environment, thus refused to be degraded in photocatalysis system. To demonstrate the stability of DPA-TiO_2, recycle experiments of MO degradation were carried out and the results are illustrated in Fig. 7(b). Obviously, this photocatalyst only shows a slightly decreased DR during repeated reactions, and it is probably caused not so much by the removal of DPA from the surface of TiO_2 as the loss in the process of catalyst recovery.

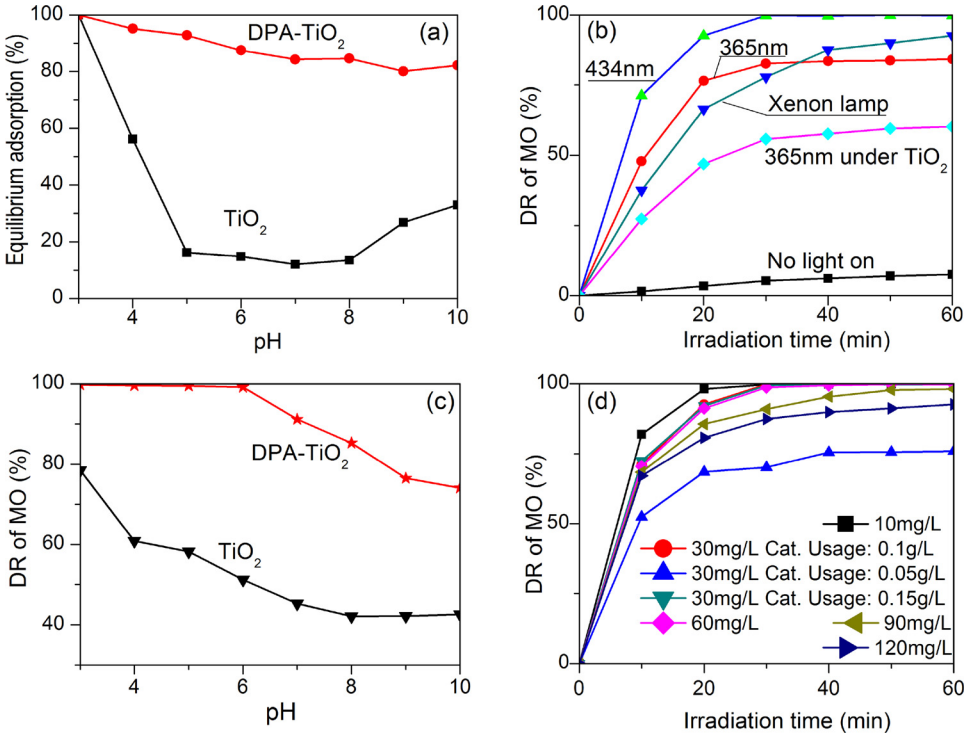

Fig. 6. Properties of catalysts TiO_2 and DPA-TiO_2. (a) Adsorption to MO under different pH. The concentration of MO aqueous solution is 10 mg/L and the usage of catalyst is 0.1 g/L. (b) Degradation rate of MO under different light sources. Each irradiation experiment was carried out at room temperature 21 ℃, and initial pH and MO concentration were 5 and 30 mg/L, respectively. (c) Degradation rate of MO under different solution pH. Each reaction was carried out for 30 min with 30 mg/L original concentration of MO and 0.1 g/L dosage of catalyst. (d) Influence of the concentration of MO and the dosage of DPA-TiO_2 on DR. The concentration of MO increases from 10 mg/L to 120 mg/L and the initial pH of these solutions was ajusted to 5. The dosage of DPA-TiO_2 is 0.1 g/L except those are indicated in picture. (For interpretation of the references to colour in the text, the reader is referred to the web version of this article.)

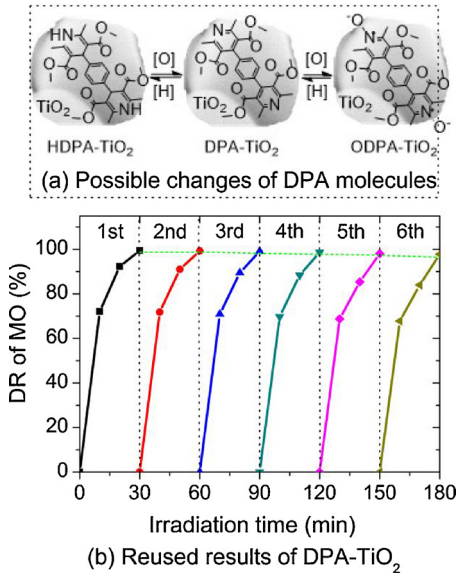

Fig. 7. The stability of DPA-TiO_2. (a) Possible structural changes of DPA molecules. (b) Degradation rate of MO under each reuse experiment of DPA-TiO_2.

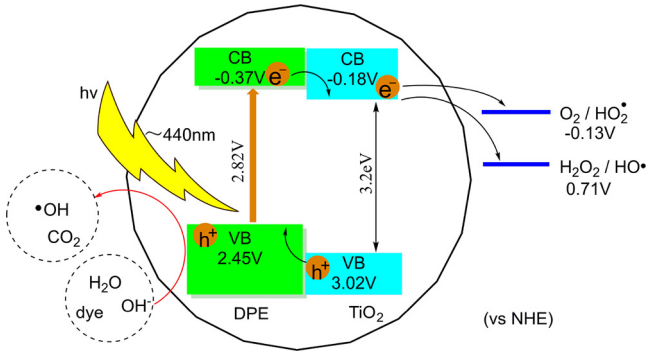

Fig. 8. Schematic diagrams showing the proposed photocatalytic mechanism of DPA-TiO_2.

3.4. Mechanism of catalysis with DPA-TiO_2

It is demonstrated that TiO_2 could be modified with organic compounds to enhance its photocatalytic activity [44,45]. The experimental results give an interesting phenomenon that TiO_2 modified with DPA exhibits excellent stability and photocatalytic activity. Base on these data and Mott-Schottky test, we present a possible mechanism as illustrated in Fig. 8. The CB and VB positions of DPE and TiO_2 indicates the matching energy levels of charges donor and acceptor. When light falls on the surface of catalyst, the new formed surface structure (as signed as DPE) of 2.82 eV bandgap is excited to give electrons [46,47], these electrons are quickly transferred to the CB of TiO_2, and then consumed by O_2 or H_2O_2 to form peroxy radicals or hydroxyl radicals, among which peroxy radicals can also react with electrons to form hydroxyl radicals [48]. Thus adding H_2O_2 undoubtedly helps the separation of photo generated charges and triggers the formation of hydroxyl radicals. On account of lacking combination with electrons, the photogenerated positive holes are easy to migrate to catalyst surface, where contact with hydroxyl ions, water or dye molecules to generate hydroxyl radicals or happen photodegradation [49–51]. In the end, the high concentration of radicals brings excellent photodegradation efficiency.

4. Conclusions

The stable organic dipyridinylbenzene DPA as modifier was successfully chem-grafted on the surface of nano-TiO_2 particles with hydrothermal reaction. The obtained organic/inorganic hybrid catalyst possesses high light absorbency and widening scope of wavelength, hence ease of producing excitons under visable irradiation. In addition, the novel catalyst exhibits excellent adsorption to waste dye molecules in a wide range of pH, which is much valuable for practical photodegradation. The high adsorption capacity can be attributed to the flexible interactions of DPA with dye molecles, which includes

electrostatic attraction, hydrogen bonds, π-π interactions and other polar interactions initiated by oxygen atoms of DPA. In addition, DPA as an electron transmitter greatly promotes the seperation of photo-excited charges, and thus remarkably increases the efficiency of photodegradation and decrease energy consumption. This hybridized catalyst has a bright prospect in the application of photocatalysis domain.

Acknowledgments

The authors acknowledge the financial support provided by Tianjin Municipal Science and Technology Commission (Scientific special commissioner project 17JCTPJC52300), and also thank Tianjin Key Laboratory of Organic Solar Cells and Photochemical Conversion for providing research facilitation and assistance.

Appendix A. Supplementary data

Supplementary material related to this article can be found, in the online version, at doi:https://doi.org/10.1016/j.apcatb.2018.03.096.

References

[1] S. Gomez, L. Lerici, C. Saux, A.L. Perez, C.D. Brondino, L. Pierella, L. Pizzio, Fe/ZSM-11 as a novel and efficient photocatalyst to degrade Dichlorvos on water solutions, Appl. Catal. B Environ. 202 (2017) 580–586.
[2] H.-Y. Jing, T. Wen, C.-M. Fan, G.-Q. Gao, S.-L. Zhong, A.-W. Xu, Efficient adsorption/photodegradation of organic pollutants from aqueous systems using Cu_2O nanocrystals as a novel integrated photocatalytic adsorbent, J. Mater. Chem. A 2 (2014) 14563.
[3] W. Raza, D. Bahnemann, M. Muneer, Efficient visible light driven, mesoporous graphitic carbon nitrite based hybrid nanocomposite: with superior photocatalytic activity for degradation of organic pollutant in aqueous phase, J. Photochem. Photobiol. A Chem. 342 (2017) 102–115.
[4] L. Yinghua, W. Huan, L. Li, C. Wenquan, Facile synthesis of Ag@AgCl plasmonic photocatalyst and its photocatalytic degradation under visible light, Rare Met. Mater. Eng. 44 (2015) 1088–1093.
[5] F. Guo, W. Shi, W. Guan, H. Huang, Y. Liu, Carbon dots/g-C3N4/ZnO nanocomposite as efficient visible-light driven photocatalyst for tetracycline total degradation, Sep. Purif. Technol. 173 (2017) 295–303.
[6] R. Xie, L. Zhang, H. Xu, Y. Zhong, X. Sui, Z. Mao, Fabrication of Z-scheme photocatalyst Ag–AgBr@Bi20TiO32 and its visible-light photocatalytic activity for the degradation of isoproturon herbicide, J. Mol. Catal. A Chem. 406 (2015) 194–203.
[7] D. Chaudhary, N. Khare, V.D. Vankar, Ag nanoparticles loaded TiO2/MWCNT ternary nanocomposite: a visible-light-driven photocatalyst with enhanced photocatalytic performance and stability, Ceram. Int. 42 (2016) 15861–15867.
[8] G. Plantard, T. Janin, V. Goetz, S. Brosillon, Solar photocatalysis treatment of phytosanitary refuses: efficiency of industrial photocatalysts, Appl. Catal. B Environ. 115–116 (2012) 38–44.
[9] C. Wang, Z. Shi, L. Peng, W. He, B. Li, K. Li, Preparation of carbon foam-loaded nano-TiO_2 photocatalyst and its degradation on methyl orange, Surf. Interfaces 7 (2017) 116–124.
[10] P. Huo, Z. Lu, X. Liu, X. Liu, X. Gao, J. Pan, D. Wu, J. Ying, H. Li, Y. Yan, Preparation molecular/ions imprinted photocatalysts of La3+@POPD/TiO_2/fly-ash cenospheres: preferential photodegradation of TCs antibiotics, Chem. Eng. J. 198–199 (2012) 73–80.
[11] F. Thevenet, O. Guaïtella, J.M. Herrmann, A. Rousseau, C. Guillard, Photocatalytic degradation of acetylene over various titanium dioxide-based photocatalysts, Appl. Catal. B Environ. 61 (2005) 58–68.
[12] O. Debono, V. Hequet, L. Le Coq, N. Locoge, F. Thevenet, VOC ternary mixture effect on ppb level photocatalytic oxidation: removal kinetic, reaction intermediates and mineralization, Appl. Catal. B Environ. 218 (2017) 359–369.
[13] P. Zhao, N. Qin, J.Z. Wen, C.L. Ren, Photocatalytic performances of ZnO nanoparticle film and vertically aligned nanorods in chamber-based microfluidic reactors: reaction kinetics and flow effects, Appl. Catal. B Environ. 209 (2017) 468–475.
[14] L. Foglia, L. Bogner, M. Wolf, J. Stähler, Localization-dependent charge separation efficiency at an organic/inorganic hybrid interface, Chem. Phys. Lett. 646 (2016) 25–30.
[15] B.Y. Lee, S.H. Park, S.C. Lee, M. Kang, S.J. Choung, Decomposition of benzene by using a discharge plasma-photocatalyst hybrid system, Catal. Today (2004) 769–776.
[16] C. Guo, S. Gao, J. Lv, S. Hou, Y. Zhang, J. Xu, Assessing the photocatalytic transformation of norfloxacin by BiOBr/iron oxides hybrid photocatalyst: kinetics, intermediates, and influencing factors, Appl. Catal. B Environ. 205 (2017) 68–77.
[17] M.M. Mohamed, I. Ibrahim, T.M. Salama, Rational design of manganese ferrite-graphene hybrid photocatalysts: efficient water splitting and effective elimination of organic pollutants, Appl. Catal. A Gen. 524 (2016) 182–191.
[18] Y. Honda, M. Watanabe, H. Hagiwara, S. Ida, T. Ishihara, Inorganic/whole-cell biohybrid photocatalyst for highly efficient hydrogen production from water, Appl. Catal. B Environ. 210 (2017) 400–406.
[19] Y. Liu, R. Wang, Z. Yang, H. Du, Y. Jiang, C. Shen, K. Liang, A. Xu, Enhanced visible-light photocatalytic activity of Z-scheme graphitic carbon nitride/oxygen vacancy-rich zinc oxide hybrid photocatalysts, Cuihua Xuebao/Chin. J. Catal. 36 (2015) 2135–2144.
[20] E. Kowalska, K. Yoshiiri, Z. Wei, S. Zheng, E. Kastl, H. Remita, B. Ohtani, S. Rau, Hybrid photocatalysts composed of titania modified with plasmonic nanoparticles and ruthenium complexes for decomposition of organic compounds, Appl. Catal. B Environ. 178 (2015) 133–143.
[21] D. Liu, M. Zhang, W. Xie, L. Sun, Y. Chen, W. Lei, Porous BN/TiO_2 hybrid nanosheets as highly efficient visible-light-driven photocatalysts, Appl. Catal. B Environ. 207 (2017) 72–78.
[22] J. Chandrasekaran, D. Nithyaprakash, K.B. Ajjan, S. Maruthamuthu, D. Manoharan, S. Kumar, Hybrid solar cell based on blending of organic and inorganic materials – an overview, Renew. Sustain. Energy Rev. 15 (2011) 1228–1238.
[23] K. Gregorczyk, M. Knez, Hybrid nanomaterials through molecular and atomic layer deposition: top down, bottom up, and in-between approaches to new materials, Prog. Mater. Sci. 75 (2016) 1–37.
[24] X. Wei, J. Liu, Nanocuboid TiO_2 based organic-inorganic hybrids for fast RhB trapping and photodegradation, Sol. Energy Mater. Sol. Cells 157 (2016) 139–145.
[25] D. Jiang, Y. Xu, D. Wu, Y. Sun, Visible-light responsive dye-modified TiO_2 photocatalyst, J. Solid State Chem. 181 (2008) 593–602.
[26] X.Y. Wu, H.X. Qi, J.J. Ning, J.F. Wang, Z.G. Ren, J.P. Lang, One silver(I)/tetraphosphine coordination polymer showing good catalytic performance in the photodegradation of nitroaromatics in aqueous solution, Appl. Catal. B Environ. 168–169 (2015) 98–104.
[27] F. Tian, R. Zhu, F. Ouyang, Synergistic photocatalytic degradation of pyridine using precious metal supported TiO_2 with $KBrO_3$, J. Environ. Sci. (China) 25 (2013) 2299–2305.
[28] L. Shen, R. Liang, L. Wu, Strategies for engineering metal-organic frameworks as efficient photocatalysts, Cuihua Xuebao/Chin. J. Catal. 36 (2015) 2071–2088.
[29] M. Wen, Y. Cui, Y. Kuwahara, K. Mori, H. Yamashita, Non-noble-metal nanoparticle supported on metal-organic framework as an efficient and durable catalyst for promoting H_2 production from ammonia borane under visible light irradiation, ACS Appl. Mater. Interfaces 8 (2016) 21278–21284.
[30] A.A. Ismail, D.W. Bahnemann, Photochemical splitting of water for hydrogen production by photocatalysis: a review, Sol. Energy Mater. Sol. Cells 128 (2014) 85–101.
[31] Z. Gan, A. Okui, Y. Kawashita, M. Hayashi, Convenient synthesis of linear-extended bipyridines involving a central phenyl linking group, Chem. Lett. 37 (2008) 1302–1303.
[32] H.J. Lee, J.H. Kim, S.S. Park, S.S. Hong, G.D. Lee, Degradation kinetics for photocatalytic reaction of methyl orange over Al-doped ZnO nanoparticles, J. Ind. Eng. Chem. 25 (2015) 199–206.
[33] Y.S. Li, J.T. Qin, Y. Han, J.F. Du, Z.B. Dong, S.F. Sun, Y. Liu, Controlled preparation and highly photocatalytic activity of portable MCC-g-GMA@TiO_2 photocatalyst by pre-radiation grafting-embedding method, Appl. Catal. B Environ. 218 (2017) 101–110.
[34] L.V. Barbosa, L. Marçal, E.J. Nassar, P.S. Calefi, M.A. Vicente, R. Trujillano, V. Rives, A. Gil, S.A. Korili, K.J. Ciuffi, E.H. De Faria, Kaolinite-titanium oxide nanocomposites prepared via sol-gel as heterogeneous photocatalysts for dyes degradation, Catal. Today 246 (2015) 133–142.
[35] L. Zhou, L. Wang, J. Lei, Y. Liu, J. Zhang, Fabrication of TiO_2/Co-g-C_3N_4 heterojunction catalyst and its photocatalytic performance, Catal. Commun. 89 (2017) 125–128.
[36] F.Z. Haque, R. Nandanwar, P. Singh, Evaluating photodegradation properties of anatase and rutile TiO_2 nanoparticles for organic compounds, Optik (Stuttg) 128 (2017) 191–200.
[37] C. Gebauer, J. Fischer, M. Wassner, T. Diemant, J. Bansmann, N. Hüsing, R.J. Behm, Novel N, C doped Ti(IV)-oxides as Pt-free catalysts for the O_2 reduction reaction, Electrochim. Acta 146 (2014) 335–345.
[38] H. Jiang, H. Song, Z. Zhou, X. Liu, G. Meng, The roles of Li^+ and F^- ions in Li-F-codoped TiO_2 system, J. Phys. Chem. Solids 68 (2007) 1830–1835.
[39] Y. Liu, R.O. Claus, Blue light emitting nanosized TiO_2 colloids, J. Am. Chem. Soc. 119 (1997) 5273–5274.
[40] C. Kormann, D.W. Bahnemann, M.R. Hoffmann, Preparation and characterization of quantum-size titanium dioxide, J. Phys. Chem. 92 (1988) 5196–5201.
[41] M.M. Dávila-Jiménez, M.P. Elizalde-González, E. García-Díaz, A.M. Santes-Aquino, Assessment of the effectiveness of combined adsorption and photocatalysis for removal of the herbicide isoproturon, Phys. Chem. Earth 91 (2016) 77–86.
[42] A.L.T. Pham, F.M. Doyle, D.L. Sedlak, Kinetics and efficiency of H_2O_2 activation by iron-containing minerals and aquifer materials, Water Res. 46 (2012) 6454–6462.
[43] V.K. Gupta, R. Kumar, A. Nayak, T.A. Saleh, M.A. Barakat, Adsorptive removal of dyes from aqueous solution onto carbon nanotubes: a review, Adv. Colloid Interface Sci. 193–194 (2013) 24–34.
[44] J.A. Rengifo-Herrera, M. Blanco, J. Wist, P. Florian, L.R. Pizzio, TiO_2 modified with polyoxotungstates should induce visible-light absorption and high photocatalytic activity through the formation of surface complexes, Appl. Catal. B Environ. 189 (2016) 99–109.
[45] E. Filippo, C. Carlucci, A.L. Capodilupo, P. Perulli, F. Conciauro, G.A. Corrente, G. Gigli, G. Ciccarella, Facile preparation of TiO_2-polyvinyl alcohol hybrid nanoparticles with improved visible light photocatalytic activity, Appl. Surf. Sci. 331 (2015) 292–298.
[46] V.I. Krinichnyi, E.I. Yudanova, V.R. Bogatyrenko, Effect of spin traps on charge transport in low-bandgap copolymer: fullerene composites, J. Phys. Chem. Solids 111 (2017) 153–159.

[47] F. Li, X. Ni, Improving poly(3-hexylthiophene)-TiO_2 heterojunction solar cells by connecting polypyrrole to the TiO_2 nanorods, Sol. Energy Mater. Sol. Cells 118 (2013) 109–115.
[48] J. Schneider, M. Matsuoka, M. Takeuchi, J. Zhang, Y. Horiuchi, M. Anpo, D.W. Bahnemann, Understanding TiO_2 photocatalysis: mechanisms and materials, Chem. Rev. 114 (2014) 9919–9986.
[49] M. Zhang, M. de Respinis, H. Frei, Time-resolved observations of water oxidation intermediates on a cobalt oxide nanoparticle catalyst, Nat. Chem. 6 (2014) 362–367.
[50] L. Yu, C. Wang, F. Chen, J. Zhang, Y. Ruan, J. Xu, Investigating the synergistic effects in tourmaline/TiO_2-based heterogeneous photocatalysis: underlying mechanism insights, J. Mol. Catal. A Chem. 411 (2016) 1–8.
[51] K. Qi, B. Cheng, J. Yu, W. Ho, Review on the improvement of the photocatalytic and antibacterial activities of ZnO, J. Alloys Compd. 727 (2017) 792–820.